CONFERENCE PRE-PRINT

EFFECT OF COLLISION PROCESSES IN DIVERTOR PLASMAS ON THE TOKAMAK OPERATIONAL WINDOW

¹D. Umezaki, ¹S. Yamoto, ²K. Hoshino, ¹N. Asakura, ¹N. Aiba

¹National Instituted for Quantum Science and Technology, Naka/Ibaraki, Japan ²Faculty of Science and Technology, Keio University, Yokohama/Kanagawa, Japan

Email: umezaki.daisuke@qst.go.jp

Abstract

The paper analyzes the impact of large-angle elastic scattering (LES) and neutral-neutral collisions (NNCs) on edge plasma transport in the JT-60SA using the integrated divertor code SONIC. The SONIC simulations were performed for the initial research-phase operation, with the exhaust power and particle flux from the core set to 18 MW and 6×10^{21} s⁻¹, respectively. To examine the operational window of the tokamak, a parametric scan was conducted for outer strike point positions, fuel gas puff rates Γ_{puff} , and the angle between the separatrix and the outer vertical target. LES drives ion transport perpendicular to the magnetic field, with velocities three to four times larger than the anomalous diffusion velocity. Its effect depends on the magnetic field direction and increases the ion density at the outer target by 10% and 18% for clockwise and counterclockwise toroidal fields as viewed from the top, respectively. Although LES has a limited impact on the peak heat load at the outer target, it shifts the peak heat load position. NNCs shorten the neutral particle mean free path, increasing molecular pressure in the sub-divertor region by 15%, thereby enhancing particle exhaust without major changes to heat loads or plasma profiles. The outer strike point position strongly influences divertor performance: lower strike points increase ion and molecular densities, decrease ion and electron temperatures, and promote recycling, reducing the peak heat load by up to 32% between extreme cases. Lower strike point positions are favorable for reducing the peak divertor heat load. The angle θ between the separatrix and the outer target slightly affects the ion density and heat loads, with shallower angles promoting heat load reduction. These improvements in the model, combined with the parametric scan, provide insights for optimizing the JT-60SA initial research phase experiments.

1. INTRODUCTION

The reduction of the heat load on the divertor target is one of the most critical challenges to achieve long time operation of future fusion devices. Detached divertor plasma has been regarded as a standard approach to maintain

a low divertor heat load. Divertor detachment requires a low electron temperature, which can be achieved thorough impurity seeding and fuel gas puffing. A number of scrape-off-layer (SOL) and divertor simulation codes, such as SOLPS 4.0 [1] and SONIC [2], have been developed. The SONIC code has been applied to prediction of the JT-60SA plasmas and JA DEMO reactor design. While the code has been applied to analyze JT-60U experiments, it has overestimated the electron density profile at the outer divertor target by a factor of 2-3 [3]. In SONIC, the plasma transport perpendicular to magnetic field lines is modeled as an anomalous diffusion assumption, addressing the need to improve the plasma transport model [3]. Our previous study [4, 5] has shown that additional plasma transport perpendicular to magnetic field lines can be driven by large-angle elastic scattering (LES) between fuel ions and fuel atoms, using a kinetic approach. Recently, a neutral-neutral collision (NNC) model utilizing a crosssection dataset derived by Krstić [6] has been implemented into the SONIC code [7, 8]. Although the effect of NNCs on particle exhaust in JT-60SA has been investigated utilizing the DIVGAS code [9], no integrated code simulation incorporating NNCs has yet been conducted for JT-60SA operations. In this study, the plasma transport model is improved by implementing LES into the SONIC code. The aim of this research is to analyze the operational window for the initial research phase of JT-60SA using the improved SONIC code, which incorporates both LES and NNC models. The analysis focuses on

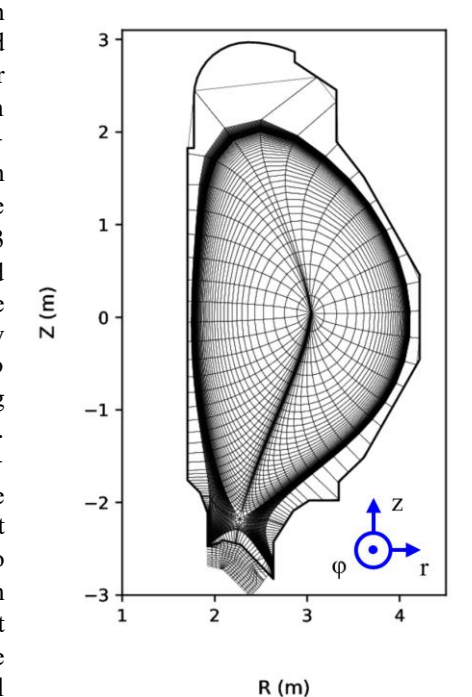


Figure 1. Computational grid of SONIC for JT-60SA.

divertor heat loads and considers parameters such as the outer strike point position, the angle between the separatrix and the outer vertical target, and the fuel gas puff rates (Γ_{puff}) .

2. ANALYSIS METHOD

2.1 SONIC code simulation

In this study, the divertor-integrated code SONIC [2] is applied to predictive simulations of the initial research-phase operation of JT-60SA [10]. This scenario aims to establish an initial development toward a baseline H-mode operation at a plasma current $I_p=4.6$ MA and a toroidal magnetic field of $B_T=2.28$ T. The SONIC code consists of the fluid plasma code SOLDOR [11], the steady-state Monte Carlo (MC) neutral transport code NEUT2D [11], and the steady-state MC impurity transport code IMPMC [12]. In this study, a simple radiation model [2] is employed to compute Ar and C impurity species radiation profiles, and the IMPMC code is not utilized. Figure 1 shows a typical JT-60SA geometry and the numerical grid used in the SONIC simulation. The fluid plasma simulations are performed for the SOL/divertor region, while MC neutral particles are traced throughout the entire region, including the sub-divertor. In this study, by adjusting currents in poloidal field coils, the strike position at the outer divertor target is modified, as explained in detail in Section 2.3. As the core-edge boundary condition, the exhaust power and particle flux are set to 18 MW and 6×10^{20} s⁻¹, respectively. Fuel D₂ gas puffing to enhance divertor recycling is applied with $\Gamma_{puff}=(5.0-20)\times10^{21}$ s⁻¹. The radiation power in the SOL/divertor region is set to 9 MW to establish divertor detachment. The transport coefficients for anomalous thermal and particle diffusion are assumed to be $\chi_i=\chi_e=1.0$ m² s⁻¹ and D=0.3 m² s⁻¹, respectively.

2.2 Models for ion transport driven by ion-atom collisions and for neutral-neutral collisions

To research the LES effect on ion transport, a new transport model is developed and implemented into the SOLDOR code. The SOLDOR code solves the Braginskii fluid equation [13] and the equation was derived utilizing the Chapman - Enskog expansion [14]. Hinton also independently arrived at the same transport coefficients [15]. By extending their discussion to ion-atom collisions, an ion transport model induced by ion-atom collisions also can be derived from the Boltzmann equation [5]. The ion flux perpendicular to the magnetic field including ion-atom collisions is written as [5, 15]:

$$n_i \overrightarrow{u_{i,\perp}} = -D \nabla n_i + \frac{\overrightarrow{F_{ia}} \times \overrightarrow{B}}{e_i B^2}, \tag{1}$$

$$\overrightarrow{F_{ia}} = -m_{ia}n_in_a(\overrightarrow{u_i} - \overrightarrow{u_a})\frac{\sqrt{2}}{3\sqrt{\pi}} \left(\frac{m_{ia}}{T_{ia}}\right)^{\frac{5}{2}} \int_0^\infty v_r^5 \sigma_{mt}(v_r) \exp\left(-\frac{m_{ia}}{2T_{ia}}v_r^2\right) dv_r. \tag{2}$$

Here, the subscripts i and a stand for ion and atom, respectively. Since this study simulates JT60SA deuterium plasmas, ions and atoms correspond to deuterons and deuterium atoms, respectively. The symbols n, e, and \vec{u} represent the density, the charge, and the flow velocity, respectively. The first term on the right-hand side of Eq. (1) represents the anomalous diffusion velocity. The terms $\overrightarrow{F_{ia}}$ and \overrightarrow{B} represent the force driven by ion - atom collisions [16] and the magnetic field, respectively. In Eq. (2), $m_{ia} (= m_i m_a / (m_i + m_a))$ and $T_{ia} (= (m_i T_i + m_a T_a) / (m_i + m_a))$ are the relative mass and the effective temperature, respectively. As discussed in Ref. [5], the differential cross section and scattering angles play crucial roles in ion transport due to ionatom collisions. The expressions in Eqs. (1) and (2) are derived from the Boltzmann equation, quantitatively considering the differential cross section through the momentum transfer cross section. NNCs have previously been implemented in the EIRENE code in advance [17]. NNCs have also been implemented in the NEUT2D code [7, 8] using cross-section datasets for neutralneutral collisions derived by Krstić [6].

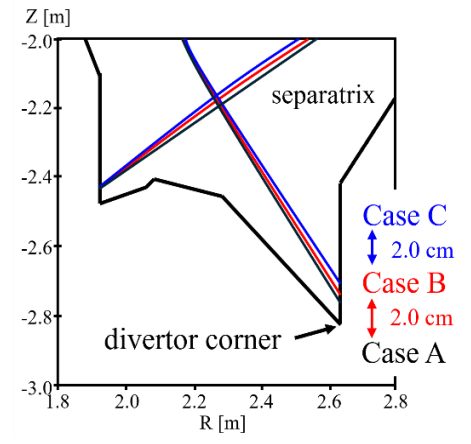


Figure 2. Positions of the outer strike points for simulation Cases A (black line), B (red line), and C (blue line).

2.3 Magnetic field configurations

In this study, SONIC simulations are performed for five different magnetic configurations. Figure 2 shows the positions of strike points for simulation Case A, B, and C. In Case A, the outer strike point is 4.5 cm above the divertor corner. In Cases B and C, the outer strike points are located 2 cm and 4 cm higher in Case A, respectively. In addition, SONIC simulations are also conducted for the magnetic field configurations with different angles between the separatrix and the outer divertor plate. These cases are based on Case B, with a shallow angle designated as Case B(-), and with a greater angle designated as Case B(+). In this study, the angle between the separatrix and the outer target is defined as $\theta = \cos^{-1}(B_r/B)$ while the other angle $\varphi = \cos^{-1}(B_z/B\cos\theta)$. Figure 3 shows the angles, and table 1 lists the angles between the separatrix and the outer target for each case.

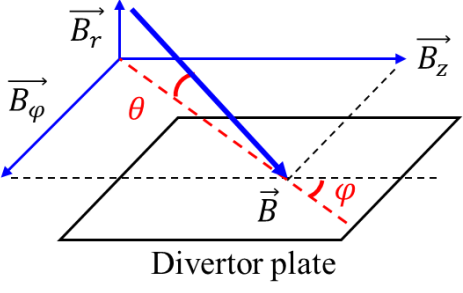


Figure 3. Definition of the angles between the separatrix and the outer target.

Tabel 1. Angles between the separatrix and the outer target for each case.

Cases	A	B(-)	В	B(+)	С
θ [°]	6.047	6.094	6.447	6.998	6.843
φ [°]	78.65	78.57	77.89	76.83	77.14

3. RESULTS AND DISCUSSION

3.1 Effects of LES and NNCs on plasma profiles and neutral pressure

In this section, we assess the effects of LES and NNCs on plasma transport and profiles.

The divertor heat load is usually more severe at the outer target. Therefore, we focus on the outer target plasma profiles. Figures 4 present (a) the typical plasma profiles and (b) the contributions to the heat flux at the outer divertor plate in Case B with LES and NNCs. In the region up to 3.4 cm, the electron temperature T_e is sufficiently reduced, indicating that partial detachment is achieved at the outer target. The peak heat load is located at the attach - detach boundary 3.3-3.4 cm.

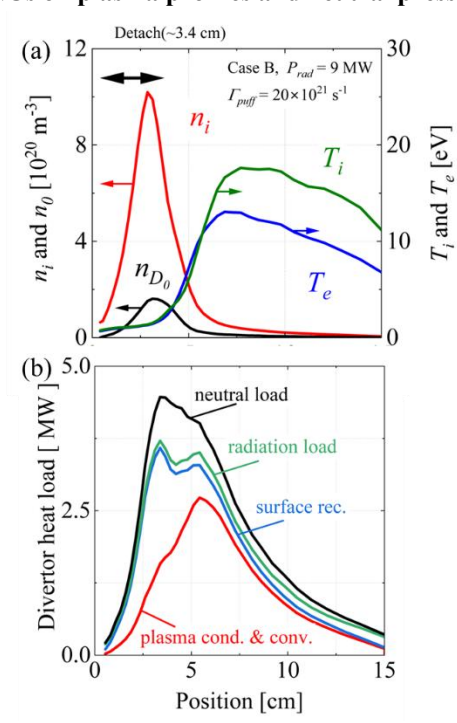


Figure 4. (a) Typical plasma profiles and (b) contributions of divertor heat load at the outer target.

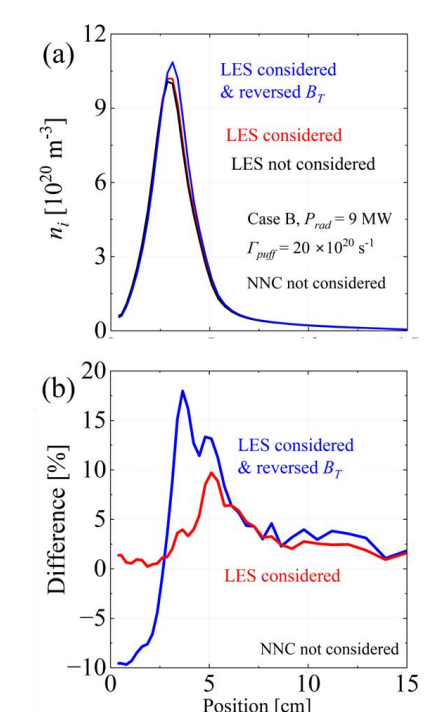


Figure 5. (a) Ion density profiles for each case and (b) density difference between the case including LES and the case excluding LES.

Next, we assess the effect of LES on plasma transport and profiles. As expected from Eqs. (1) and (2), the ion velocity V_{LES} driven by LES increases with atom density and temperature. The velocity V_{LES} reaches 40

m/s around the attach-detach boundary (3.4–3.6 cm) at the outer target, whereas the anomalous diffusion velocity V_d is only about 10 m/s near the boundary. Thus, V_{LES} can be three to four times larger than the anomalous diffusion velocity near the divertor target. Figures 5 show (a) the density profiles at the outer target and (b) the density differences between the case including LES and the case excluding LES. In figure 5(a), the black line excludes LES, while the red and blue lines include LES for the clockwise and counterclockwise toroidal magnetic fields as viewed from the top, respectively. For JT-60SA, the clockwise toroidal field is the standard configuration, whereas the counterclockwise field represents the reversed configuration. When LES is considered, the ion density increases, and the peak difference reaches 10%. With the reversed toroidal field, the difference increases to 18%. LES induces ion transport perpendicular to the magnetic field, thereby modifying the plasma profiles at the outer target. As expressed in Eq. (1), the direction of the LES-driven velocity depends on both the magnetic field direction and the neutral flow velocity. For the reversed field case, the density difference due to LES is pronounced at the attach-detach boundary, implying that LES can affect the assessment of divertor detachment. However, under the simulation conditions, the impact of LES on the peak heat load is small. The peak heat load is 4.30 MW m⁻² without LES (the black line in figure 5(a)), 4.23 MW m⁻² with LES (the red line), and 4.33 MW m⁻² with LES at the reversed magnetic field (the blue line). Although the magnitude of the peak heat load changes only slightly, the contributions to the peak heat load vary significantly when LES is considered. While the heat load due to plasma conduction and convection decreases, the contribution from surface recombination increases. As LES alters the profile of heat load contributions, the location of the peak heat load also shifts. The peak positions are 4.02 cm without LES, 3.38 cm with LES, and 3.65 cm with LES under the reversed magnetic field. Therefore, LES may affect the assessment of divertor detachment and heat load profiles.

Here, we discuss the effect of NNCs on neutral pressure. Figures 6 present (a) the atom pressure and (b) the molecular pressure in the sub-divertor region. The pressures at the three points indicated in the figure are also plotted. When NNCs are considered, the mean free path of neutral particles is shortened. As a result, atoms remain near the divertor plate, leading to a reduction of the atom pressure P_{D^0} in the sub-divertor region, as shown in figure 6(a). In contrast, the molecular pressure in the sub-divertor region increases by approximately 15%. This indicates improved particle exhaust, and consequently, greater accuracy in future He simulations is anticipated. We also evaluate the impact of NNCs on outer divertor plasma profiles. In all cases, because NNCs slightly modify the profiles of neutral particles and ionization reactions, the ion density at the outer target decreases slightly. Due to this reduction in ion density, the plasma temperature increases, and the peak heat load also increases slightly. However, the difference in the peak heat load is small; for example, in the case shown in figure 4, it is 4.5%. Therefore, in this JT-60SA operation scenario, where sufficient power is radiated, NNCs do not significantly affect the divertor heat load or plasma profiles, while an improvement in particle exhaust is expected.

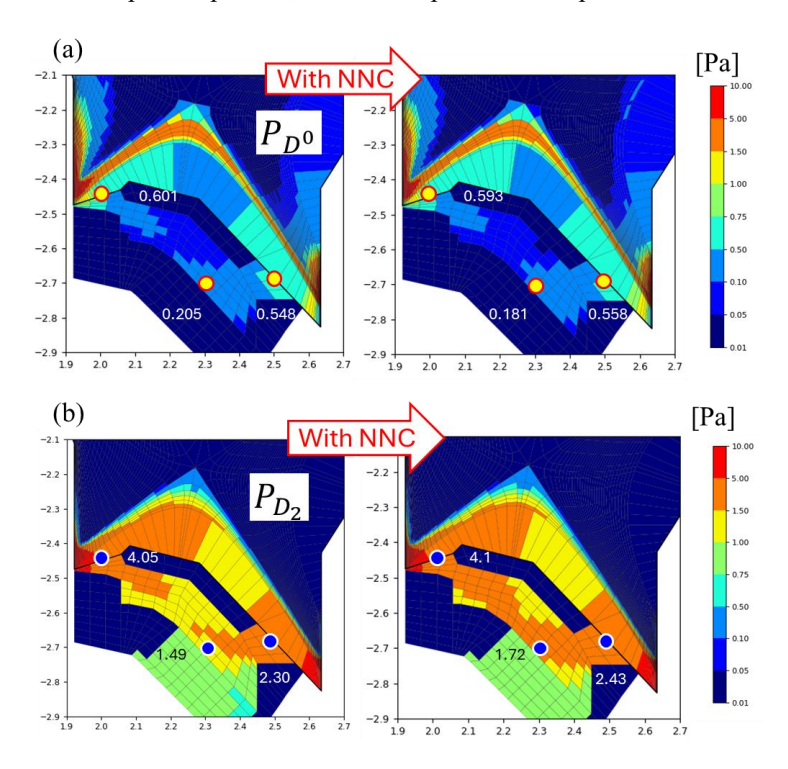


Figure 6. (a) Atomic pressure and (b) molecular pressure profiles in the sub-divertor region.

3.2 Effect of the outer strike point position

In this section, we assess the effect of the outer strike point position. Figures 7 present (a) the ion density, (b) the atom and molecular densities, (c) the ion temperature, and (d) the electron temperature profiles calculated for Cases A, B, and C, considering LES and NNCs at $\Gamma_{puff} = 20 \times 10^{21} \, \text{s}^{-1}$ and $P_{rad} = 9 \, \text{MW}$. Partial detachment is established in all cases. The lower the strike point, the larger the increase in ion and molecular densities, and the lower the ion and electron temperatures. In the lower strike point cases, divertor recycling is promoted more efficiently. However, the dependence of the peak atom density on the strike point position is small. Figure 8 shows the dependence of the peak heat load on Γ_{puff} for each case. The lower the strike point, the smaller the heat load; when $\Gamma_{puff} = 20 \times 10^{21} \, \text{s}^{-1}$, the difference between Case A (3.82 MW/m²) and Case C (5.03 MW/m²) is as large as approximately 32%. A gas puff rate $\Gamma_{puff} \geq 10 \times 10^{21} \, \text{s}^{-1}$ is required to maintain the peak divertor heat load below 10 MW m² for each simulation case.

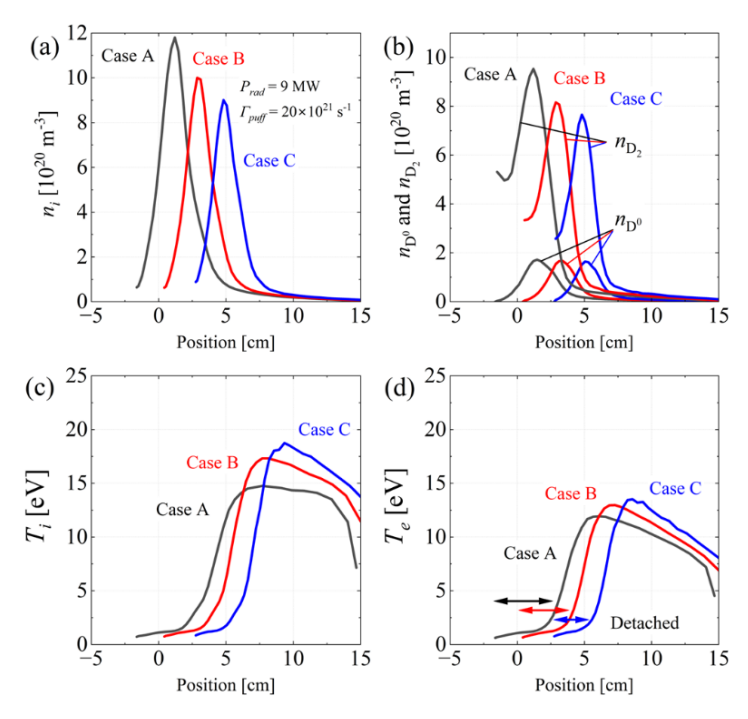


Figure 7. (a) Ion density, (b) molecular and atomic densities, (c) ion temperature, and (d) electron temperature profiles for Cases A (black line), B (red line), and C (blue line).

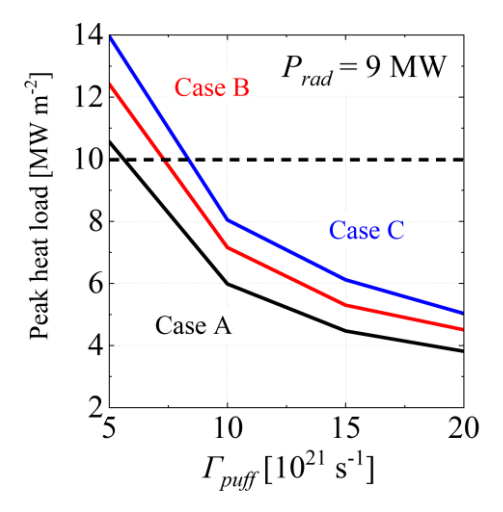


Figure 8. Dependence of the peak heat load on the gas puff rate (Γ_{puff}) at the outer target for each case.

3.3 Effect of the angle between the separatrix and the outer target

In this section, the effect of the separatrix angle with respect to the divertor plate on plasma transport is assessed. Figure 9 shows the ion density profiles at the outer target calculated for Cases B(-), B, and B(+). In these simulations, both LES and NNCs are considered. As shown in figure 9, the ion density increases as the angle θ between the separatrix and the outer vertical target decreases. The positions of the density peaks are almost unchanged with varying angle. However, the difference in the peak density between the lowest–angle case B(-) and the highest–angle case B(+) is only about 6.1%. The peak heat loads at the outer target for Cases B(-), B, and B(+) are approximately 4.26, 4.51, and 4.69 MW m⁻², respectively. The difference between B(-) and B(+) reaches approximately 10.1%. Figure 10 also shows the breakdown of the contributions to the peak heat load at the outer divertor target for each case. In all cases, plasma conduction, convection, and surface recombination are the dominant contributions. The contributions from plasma conduction convection, surface recombination, and the neutral load all increase with increasing θ . In contrast, although the radiation load decreases with increasing θ , its contribution to the peak heat load remains small. A shallower angle relative to the divertor plate increases the wetted surface area, thereby reducing the peak heat load.

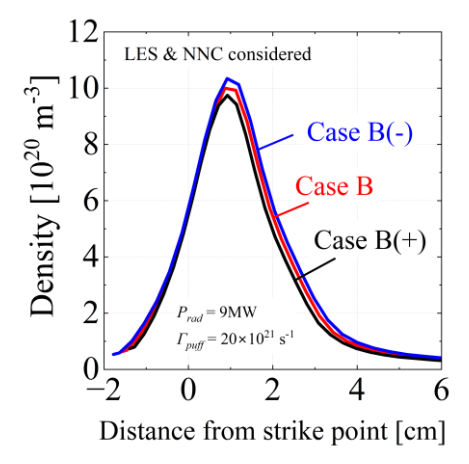


Figure 9. Density profiles at the outer target for each case.

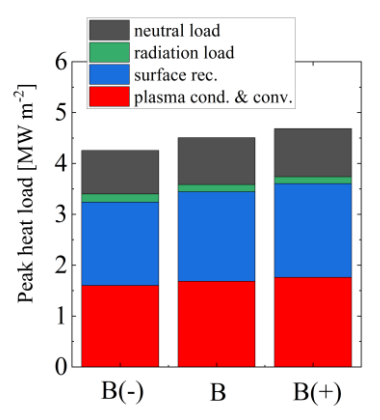


Figure 10. Contributions to the peak heat load at the outer divertor target for each case.

Next, the effect of the angle θ on LES and NNCs is assessed. Figures 11(a) and (b) show the change ratios of the peak heat load when LES and NNCs are considered, relative to the case without either effect. Figure 11(a) corresponds to $\Gamma_{puff} = 20 \times 10^{21} \, \mathrm{s}^{-1}$, and figure 11(b) to $\Gamma_{puff} = 10 \times 10^{21} \, \mathrm{s}^{-1}$. When LES is included, the peak heat load is reduced, and the reduction ratio increases at lower Γ_{puff} . On the other hand, NNCs increase the peak heat load, and when both LES and NNCs are included, the change ratio can be explained as the sum of their effects. The influence of NNCs on the change ratio appears to be independent on the leg angle θ . Although the effect of LES also seems only weakly dependent on the leg angle θ , a shallower angle, such as in Case B(-), is more favorable for reducing the heat load through LES.

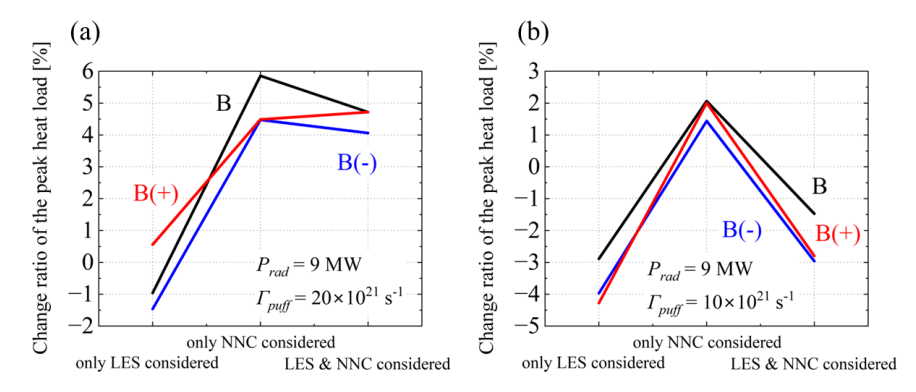


Figure 11. (a) Change ratio of the peak heat load at the outer target when LES and NNCs are considered, relative to the case without these effects, for each case.

4. CONCLUSION

In this study, as a physical model update, large-angle elastic scattering (LES) between ions and atoms is incorporated into the SONIC code. For an accurately assessment of the effect of LES, a new ion transport model is developed by extending the model derived Braginskii and Hinton based on the Boltzmann collision integral. A neutral-neutral collision (NNC) model was also implemented as a recently update. Using the improved SONIC code, the fundamental effect of LES and NNCs on ion transport and plasma profiles was investigated. Moreover, the operational window for the initial research phase of JT–60SA was analysed. The analysis particular focuses on the outer divertor heat load and considers parameters such as the outer strike point position, the angle between the separatrix and the outer target, and the fuel gas puffing rate.

First, the effect of LES on ion transport and the density profile is analysed. At the JT-60SA outer divertor target, LES induced the ion transport perpendicular to the magnetic field, which can reach three to four times larger than the anomalous diffusion velocity. As the LES velocity is driven in the direction of cross product of the atom flow velocity and the magnetic field, the dependence of the LES effect on the magnetic field direction was also assessed. LES increased the ion density near the strike point at the outer target by 10% and 18% in the clockwise and counterclockwise magnetic fields as viewed from the top, respectively. Although the effect of LES on the peak heat load was small, the position of the peak heat load was shifted by LES. Next, the effect of NNCs on the neutral pressure in sub–divertor region was investigated. By considering NNCs, the mean free path of neutral particles was shortened, thus the molecular pressure in the sub–divertor region was increased by 15%. Therefore, in this JT–60SA operation scenario, NNCs do not significantly affect the divertor heat load or plasma profiles, while an improvement in particle exhaust is expected.

The effect of the outer strike point position on the divertor heat load was also examined by simulating the three magnetic field configurations: Cases A, B, and C. In Case A, the outer strike point is located 4.5 cm above the divertor corner, while in Cases B and C, the outer strike points are 2 cm and 4 cm higher than in Case A, respectively. The lower the strike point, the greater the increase in ion and molecular densities, and the lower the ion and electron temperatures. In the lower strike point cases, divertor recycling is promoted more efficiently. The lower the strike point, the smaller the heat load; when $\Gamma_{puff} = 20 \times 10^{21} \text{ s}^{-1}$, the difference between Case A (3.82 MW/m²) and Case C (5.03 MW/m²) reaches approximately 32%. The effect of the angle θ between the separatrix and the outer divertor target was also assessed by simulating for three Cases B(-), B, and B(+) at $\theta = 6.094^{\circ}$, 6.447° , and 6.998° , respectively. The ion density at the outer divertor increases slightly as θ decreases. The peak heat loads at the outer target for Cases B(-), B, and B(+) are approximately 4.26, 4.51, and 4.69 MW m⁻², respectively; thus, the difference between B(-) and B(+) reaches approximately 10.1%. The effect of θ on LES and NNCs was also examined. When LES is included, the peak heat load is reduced, and the reduction ratio increases at lower Γ_{puff} . In contrast, NNCs increase the peak heat load, and when both LES and NNCs are included, the resulting change ratio can be explained as the sum of their individual effects. Although the effect of LES is only weakly dependent on the leg angle θ , a shallower angle, such as in Case B(-), is more favorable for reducing the heat load through LES.

REFERENCES

- [1] A. S. Kukushkin, et al., Fusion Eng. Des. (2011), 86, 2865.
- [2] H. Kawashima, et al., Plasma Fusion Res. (2006), 1, 31.
- [3] K. Hoshino J. Nucl. Mater. (2015), 463, 573.
- [4] D. Umezaki, et al., Conntrib. Plasma Phys. (2024), 64(1), e202300064.
- [5] D. Umezaki and K. Yanagihara, Conntrib. Plasma Phys. (2025), e70025.
- [6] P. S. Krstić and D. R. Schultz, At. Plasma-Mat. Interact. Data Fusion (1992), 8, 1.
- [7] S. Tokunaga, et al., 22nd International Conference on Plasma Surface Interactions in Controlled Fusion Devices, P.3.105, May (2016), Rome, Italy.
- [8] K. Hoshino, et al., the 18th International Workshop on Plasma Edge Theory in Fusion Devices, Session1-7, Sep., (2021).
- [9] C. Day, et al., the 26th IAEA Fusion Energy Conference, October (2016), Kyoto, Japan.
- [10] JT-60SA Research Plan, Research Objectives and Strategy Version 4.0, (2018), http://www.jt60sa.org/pdfs/JT-60SA Res Plan.pdf
- [11] K. Shimizu, et al., J. Nucm. Mater. (2003), 313-316, 1277-1281.
- [12] K. Shimizu, et al., J. Nucl. Mater. (1995), 220-222, 410-414.

IAEA-CN-316/2801

[Right hand page running head is the paper number in Times New Roman 8 point bold capitals, centred]

- [13] S. I. Braginskii, Transport Processes in a Plasma. in Reviews of Plasma Physics, Vol. 1 (Ed: M. A. Leontovich), Consultants Bureau, NY (1965).
- [14] S. Chapman and T. G. Cowling, The Mathematical Theory of Non-uniform Gases. 3rd edition, Cambridge university press, (1970).
- [15] F. L. Hinton, Collisional transport in plasma. in Handbook of Plasma Physics, (1983), 1, 147.
- [16] V. E. Golant, A. P. Zhilinskii, and I. E. Sakharov, "Foundations of plasma physics", (Atomizdat, Moscow, 1977); Japanese translation (1983).
- [17] D. Reiter, J. Nucl. Mater. (1992), 196-198, 80-89.